

Artificial Neural Networks (ANN) of Proposed Linear Induction Motor with Hybrid Secondary (HLIM) Considering the End Effect

¹Arash Mousaei, ¹Nasim Bahari and ²Guo Miehao

¹Department of Electrical and Computer Engineering, University of Tabriz, Tabriz, Iran

²Department of Electrical and Computer Engineering, University of Michigan, East Lansing, Michigan, USA

Key words: Linear Induction Motors (LIMs), Hybrid secondary, Direct Thrust Force Control (DTFC), Particle Swarm Optimization (SPO)

Corresponding Author:

Arash Mousaei

Department of Electrical and Computer Engineering,
University of Tabriz, Tabriz, Iran

Page No.: 85-92

Volume: 14, Issue 6, 2020

ISSN: 1990-7958

International Journal of Electrical and Power Engineering

Copy Right: Medwell Publications

Abstract: Now a days, linear electric motors are used in industries and applications that require linear motion. Different classifications for linear motors can be considered that one of them is based on their secondary. They have two secondary types: Flat (FLIM) and Ladder (LLIM) secondary. LLIMs have more thrust force than FLIMs, however due to their higher design cost, they are less popular. In this study we proposed a linear induction motor with Hybrid (HLIM) secondary and its relationships with consideration of the end effect. Then, this motor optimally designed using the Particle Swarm Optimization (PSO) algorithm. Next its output speed is controlled by the Direct Thrust Force Control (DTFC) method. According to the results, speed of HLIM reaches the desired speed in less time than and also less ripple than LLIM and FLIM. Also, HLIM has more power factor as well as more thrust force and more efficiency than LLIM and FLIM. Also, HLIM has less design cost than the LLIM and FLIM.

INTRODUCTION

Linear Induction Motors (LIMs) are a subset of electric machines that linear speed and force are generated by magnetic fields and unlike rotary electric motors, do not require mechanical devices to convert rotary motion into linear motion. Linear motors have been of much interest to researchers over the past 40 years and many articles have been written on their existing phenomena. By Mousaei *et al.*^[1], a special Linear Induction Motor with Hybrid secondary (HLIM) is designed for Textile application. By Shadabi *et al.*^[2], a LIM is controlled by an improved Direct Thrust Force Control (DTFC) where by optimizing the PI controller, its speed reaches reference speed with less ripple than the non-optimized mode. The End-effect is one of the most important phenomena in

LIM that effects the performance of the motor. By Yamazaki^[3], Shiri and Sholai^[4], Amiri and Mendrela^[5], Laithwaite and Nasar^[6], Shiri and Shoulai^[7], Yu and Fahimi^[8], Woronowicz and Safae^[9], this phenomenon is studied and parameters of the motor are obtained considering it. By Sarapulov *et al.*^[10] an equivalent circuit of π shape is presented and the parameters of the motor are calculated. By Zare-Bazghaleg *et al.*^[11] and Isfahani *et al.*^[12], the motor design and optimization are discussed with different optimization methods and considering different objective functions.

Mostly cites articles focused on Linear Induction Motors with Flat (FLIMs) secondary while Linear Induction Motor with Ladder (LLIMs) secondary can be better in some applications. By Hofmann *et al.*^[13], the End-effect in LLIM is studied. By Fujii and Harada^[14], a

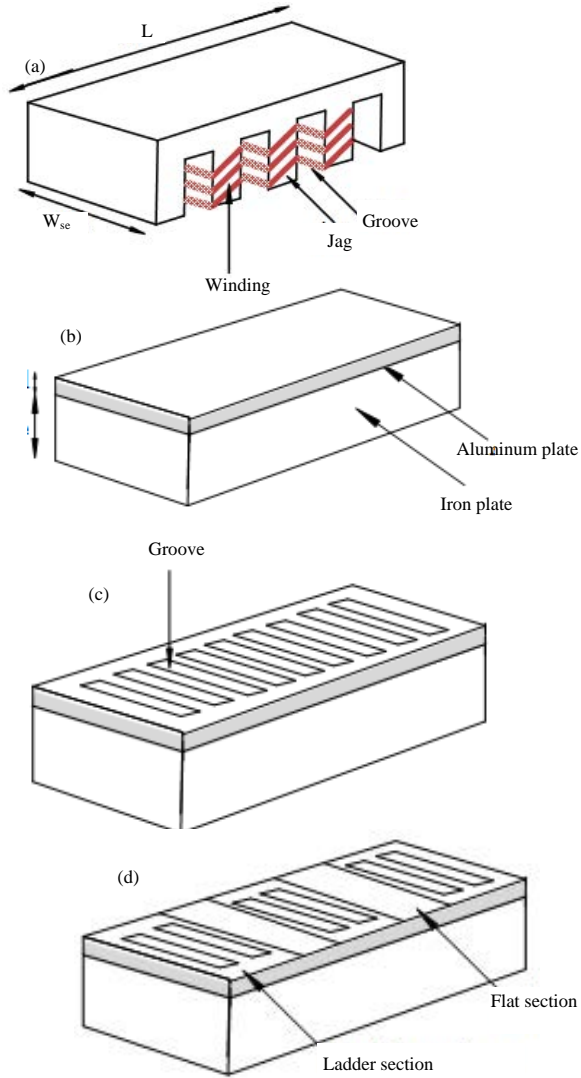


Fig. 1 (a-d): Linear induction motor, (a) Primary, (b) Flat and (c) Hybrid secondary

special form of secondary bars is considered that improves the motor performance and increases its thrust force. By Yamaguchi and Matsui^[15], a new method is presented for modelling a LLIM based on its magnetic equivalent circuit. By Naderi and Shirj^[16] with respect to the end effect, the linear induction motor is optimized and by oblique secondary bars the ripple flux density is reduced.

By Kazraji *et al.*^[17], the Fuzzy Predictive Force Control (FPFC) for speed sensor less control of single-side Linear Induction Motor. The results showed that this control method has better performance in comparison to the conventional predictive control method. By Holakooie *et al.*^[18], the MRAS strategy control is examined and Results indicated that the proposed adaptation mechanisms improve performance of MRAS

speed estimator. By Lin *et al.*^[19], a FPGA-based method is presented where with the adaptive back stepping sliding-mode controller, the mover position of the FPGA-based LIM drive possesses the advantages of good transient control performance and robustness to uncertainties in the tracking of periodic reference trajectories.

Due to the above articles has been less discussion about the DTFC method for HLIM. In this paper, we first reviewed, simulated and optimized a HLIM using the Particle Swarm Optimization (PSO) algorithm^[20] and its speed will be controlled by the DTFC and will be compared with two types of LLIM and FLIM. Then its output thrust force will be compared with two types of LLIM and FLIM. According to the results, the HLIM thrust force is more than FLIM and LLIM. Also, HLIM reaches the desired speed in less time than as well as less ripple than FLIM and LLIM. As well as according to the results HLIM has a higher power factor, higher thrust force and efficiency than LLIM and FLIM. MATLAB© Software is used to check the results.

Relationship of HLIM, LLIM and FLIM: Figure 1 shows LLIM and FLIM. In Fig. 1a, L and W_{se} are the primary length and the primary width, respectively. In Fig. 1b-d is the thickness of aluminum sheet and h_{se} is the thickness of iron sheet. For both types of flat and ladder secondary induction motors, the values of primary resistance and reactance as well as magnetization reactance are equal. Primary resistance and reactance are obtained from the following equations^[4] (Fig. 2).

$$R_1 = \rho \frac{2N(L.W_{se})}{A} \quad (1)$$

$$X_1 = \frac{12.56f.N^2 \left[\left(\lambda_s \left(1 + \frac{3}{2P} \right) + \lambda_d \right) \frac{W_{se}}{q} + \lambda_e.L \right]}{P} \quad (2)$$

Where:

N = The number of primary coils

A = Cross sectional of winding

ρ = Resistance of primary coils

f = Frequency

P = The number of pole pairs

λ_s = The groove specific magnetic conductivity

λ_e = The magnetic conductivity of the end joints

λ_d = The differential magnetic conductivity

q = The number of grooves per motor phase that calculated as follows:

$$\lambda_s = \mu_0 \frac{h_s(1+3\beta)}{12W_{se}} \quad (3)$$

$$\lambda_s = 0.3\mu_0(3\beta-1) \quad (4)$$

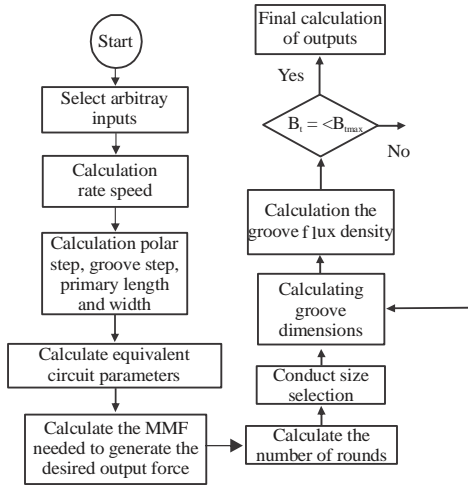


Fig. 2: Block design of optimization algorithm

$$\lambda_d = \mu_0 \frac{5g_{ei}}{5W_{se} + 4g_{ei}} \quad (5)$$

$$\lambda_d = \mu_0 \frac{5g_{ei}}{5W_{se} + 4g_{ei}} \quad (6)$$

Where:

- β = Step of winding to step of polar
- g_{ei} = Effective length of air gap
- h_s = Depth of primary groove
- m = The number of phases
- z = The total number of groove

Also, for calculate the magnetization reactance, the following equation is used:

$$x_m = \frac{37.7f\mu_0 W_{se} K_w^2 N^2 \tau}{m^2 P g_{ei}} \quad (7)$$

where, K_w is the coefficient of winding and calculated using following relations:

$$K_w = K_p K_d \quad (8)$$

$$K_p = \sin\left(\beta \frac{\pi}{2}\right) \quad (9)$$

$$K_d = \frac{\sin\left(q \frac{\alpha}{2}\right)}{q \sin\left(\frac{\alpha}{2}\right)} \quad (10)$$

where, α is the electric angle of the groove in terms of electrical degree and we have:

$$\alpha = \frac{2\pi P}{z} \quad (11)$$

For resistance of secondary in FLIM we have:

$$R_{2FILM} = \frac{6W_{se} K_w^2 N^2}{P \tau \sigma_{ei} d} \quad (12)$$

That σ_{ei} is the secondary conductivity that equivalent to:

$$\sigma_{ei} = \frac{\sigma}{k_{sk} k_{tr}} + \frac{\sigma_i \delta_i}{k_{tr} d} \quad (13)$$

Where:

- k_{sk} = Coefficient of secondary conductivity
- k_{tri} = Coefficient of iron conductivity due to the edge effect
- δ_s and δ_i = The depth of field penetration in aluminum and secondary iron, respectively, obtained from the following equations:

$$k_{sk} = \frac{d}{\delta_s} \left[\frac{\sinh\left(\frac{2d}{\delta_s}\right) + \sinh\frac{2d}{\delta_s}}{\cosh\left(\frac{2d}{\delta_s}\right) - \cosh\frac{2d}{\delta_s}} \right] \quad (14)$$

$$k_{sk} = \frac{d}{\delta_s} \left[\frac{\sinh\left(\frac{2d}{\delta_s}\right) + \sinh\frac{2d}{\delta_s}}{\cosh\left(\frac{2d}{\delta_s}\right) - \cosh\frac{2d}{\delta_s}} \right] \quad (15)$$

$$\delta_i = \text{Re} \left[\frac{1}{\sqrt{\left(\frac{\pi}{\tau}\right)^2 + j \frac{\omega \mu_{ri} \mu_0 s}{k_{tri}}}} \right] \quad (16)$$

$$\delta_i = \text{Re} \left[\frac{1}{\frac{1}{2} \sqrt{\left(\frac{\pi}{\tau}\right)^2 + \mu_0 \pi f s \sigma}} \right] \quad (17)$$

That σ is the secondary aluminum conductivity, σ_i is the secondary iron conductivity, k_{tr} is a constant coefficient that depends on the motor quality and μ_{ri} is the relative magnetic permeability coefficient of the secondary iron. In FLIM, secondary inductance can be ignored. In the other words:

$$X_{2FILM} \approx 0 \quad (18)$$

In LLIM the secondary resistance will be as follows:

$$R_{2LIM} = \frac{W_{se} N^2 K_w^2 \tau^2 A_s}{P \tau d W_2 \sigma} (1 + A_e) \quad (19)$$

Where:

- τ_2 = The secondary groove step
- A_s = The cross-sectional of the secondary groove
- A_e = A coefficient of resistance between the secondary grooves and obtained from the following relation:

$$A_e = \frac{R_{s2}}{2R_b \sin^2 \left(\frac{\pi P}{N_1} \right)} \quad (20)$$

Where:

- R_2 = The resistance of between of ladder
- R_b = The resistance of ladder
- N_1 = The number of grooves in the secondary.

Also, in LLIM, the secondary reactance is not zero and calculated as follows:

$$X_2 = 150.8\mu_0 W_{se} N_1 K_w^2 f (\lambda_{s2} + \lambda_{e2} + \lambda_{d2}) \quad (21)$$

That λ_{d2} , λ_{e2} and λ_{s2} are the differential magnetic conductivity, end connections conductivity and the secondary groove conductivity, respectively^[14]. According to the mentioned relations, for secondary resistance and reactance of proposed HLIM, we will have:

$$R_{2HLIM} = GR_{2FLIM} + HR_{2LLIM} \quad (22)$$

$$X_{2HLIM} = GX_{2FLIM} + HX_{2LLIM} \quad (23)$$

where, G and H, are Flat section and Ladder section length, respectively.

Dynamic Model of HLIM: In order to obtain the HLIM model in a d-q reference frame, first the stator voltage equation should be introduced:

$$U_{ds} = R_1 i_{ds} + R_{2HLIM} f(Q) (i_{ds} + i_{dr}) + \frac{d\lambda_{ds}}{dt} - \omega_c \lambda_{qs} \quad (24)$$

$$U_{qs} = R_1 i_{qs} + \frac{d\lambda_{qs}}{dt} + \omega_c \lambda_{ds} \quad (25)$$

$$U_{dr} = R_{2HLIM} i_{dr} + \frac{d\lambda_{dr}}{dt} - (\omega_c - \omega_r) \lambda_{qs} \quad (26)$$

$$U_{qr} = R_{2HLIM} i_{qr} + \frac{d\lambda_{qr}}{dt} + (\omega_c - \omega_r) \lambda_{dr} \quad (27)$$

$$\lambda_{ds} = L_1 i_{ds} + L_m (1-f(Q)) (i_{ds} + i_{dr}) \quad (28)$$

Table 1: Rated motor input values

Specifications	Amounts
Voltage (V)	220
Thrust force (N)	30
Frequency (Hz)	50
Speed (m sec)	2
Slip	0.2
Voltage (V)	220
Thrust force (N)	30

Table 2: Output values for optimal design of HLIM

Specifications	Amounts
Effective air distance	3.21 mm
Number of pair poles	2
Iron secondary thickness	15.9 mm
Primary length	0.629 m
Secondary length	0.8 m
Secondary groove Width	5.2 mm
Primary groove width	5.5 mm
Frequency	50
Number of rounds	316
Number of grooves in each phase at each pole	3
Primary width	106.48 mm
Secondary width	130.73 mm
Secondary jag Width	8.3 mm
Primary jag width	3 mm
m	51
Primary groove depth	34.17 mm
H	7.74 mm

$$\lambda_{qs} = L_1 i_{qs} + L_m (i_{qs} + i_{qr}) \quad (29)$$

$$\lambda_{dr} = L_{2HLIM} i_{qr} + L_m (1-f(Q)) (i_{ds} + i_{dr}) \quad (30)$$

$$\lambda_{qr} = L_{2HLIM} i_{qr} + L_m (i_{qs} + i_{qr}) \quad (31)$$

$$f(Q) = \frac{1-e^{-Q}}{Q} \quad (32)$$

$$Q = \frac{(nG+mh)}{VL_{2HLIM}} R_{2HLIM} \quad (33)$$

In the above relationships, n is number of flat sections and m is number of ladder sections. According to relationships Eq. 5, 6 and 16 we have (Table 1 and 2):

$$Q = \frac{(nG + mH)(GR_{2FLIM} + HR_{2LLIM})}{V(GL_{2FLIM} + HL_{2LLIM})} \quad (34)$$

After solving the above relationship, we have:

$$\frac{dQ}{dt} = -\frac{1}{V^2(GL_{2FLIM} + HL_{2LLIM})} (nG^2 R_{FLIM} + \quad (35)$$

$$nHR_{LLIM} + mHGR_{FLIM} + mH^2 R_{LLIM}) \frac{dV}{dt}$$

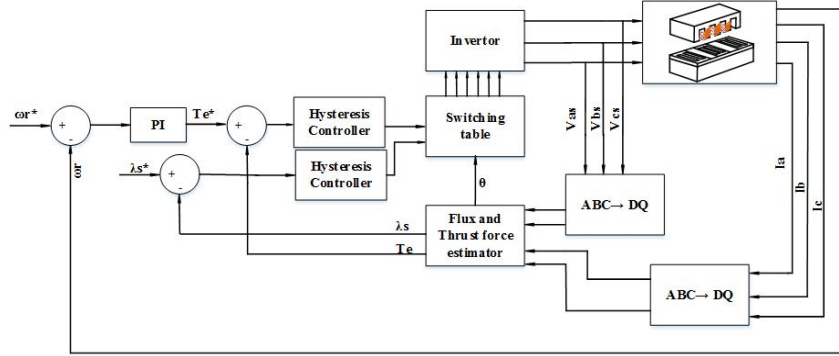


Fig. 3: Block diagram of DTFC

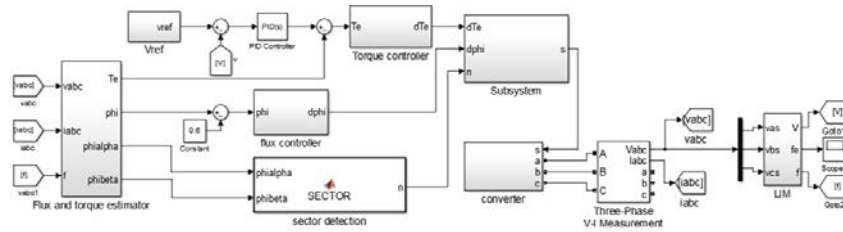


Fig. 4: Simulink model of DTFC for HLIM with end effects

Table 3: Switch table

Error status of	θ(1)	θ(2)	θ(3)	θ(4)	θ(5)	θ(6)
$\lambda = 1$						
$T_e = 1$	2	3	4	4	6	1
$T_e = 0$	0	7	0	7	0	7
$T_e = -1$	6	1	2	3	4	5
$\lambda = 0$						
$T_e = 1$	5	6	1	2	3	4
$T_e = 0$	7	0	7	0	7	0
$T_e = -1$	5	6	1	2	3	4

Optimization and design: The Particle Swarm Optimization (PSO) algorithm^[20] is used to design and optimize the motor. In this algorithm, arbitrary inputs are first given and based on the condition that we place at the end of the algorithm, equivalent circuit parameters of motor are design and obtained. Here, first, inputs such as voltage, frequency, rated speed and rated slip are considered. Then, according to the following algorithm, the required outputs for the motor design are calculated: The following table shows the rated inputs for FLIM and LLIM:

According to the values Table 1 and the proposed algorithm, the optimal values for the design of the linear induction motor are given in the following tables. Various variables can be considered to optimize the design. The following (Table 2) values are obtained with consider the output power, speed and efficiency of the motor as objective function.

Direct thrust force of HLIM: In the Direct Thrust Force Control (DTFC) method, speed and stator voltage of motor are calculated by the sensor^[2]. Then by

relationships (Eq. 36-40), the flux linkage, θ and thrust force are estimated. Next, compared with real and reference value of the flux linkage and thrust force. Then they are passed through the hysteresis controllers. Then using the switching (Table 3) for selection the inverter's switch on and off to provide the demand voltage. Figure 3 and 4 shows the DTFC method:

$$F_c = \frac{3p\pi C}{4\tau} \frac{L_m(1-f(Q))}{L_{2HLIM} - H_m f(Q)} \left(\lambda_{dr} i_{qs} - L_{2HLIM} \frac{f}{1-f} i_{qs} i_{ds} = m \frac{dV}{dt} + BV + F_L \right) \quad (36)$$

$$F_c = \frac{3p\pi C}{4\tau} \frac{L_m(1-f(Q))}{L_{2HLIM} - H_m f(Q)} \left(\lambda_{dr} i_{qs} - L_{2HLIM} \frac{f}{1-f} i_{qs} i_{ds} = m \frac{dV}{dt} + BV + F_L \right) \quad (37)$$

$$\lambda_{qs} = \int (U_{qs} - R_1 i_{qs}) dt \quad (38)$$

$$\lambda_{qs} = \sqrt{\lambda_{ds}^2 + \lambda_{qs}^2} \quad (39)$$

$$\theta = \tan^{-1} \tan^{-1} \left(\frac{\lambda_{qs}}{\lambda_{ds}} \right) \quad (40)$$

RESULTS AND DISCUSSION

In this study, simulation results of HLIM, LLIM and FLIM will be presented. The main aim of this study is

Table 4: Output values for optimal design of LLIM

Specifications	Amounts
Width of Primary jag	4 mm
Primary groove width	5.7 mm
Groove depth	21.3 mm
Groove width to step ratio	0.6365
Secondary iron thickness	14.6 mm
Motor length	0.3 m
Number of secondary bars	218
Secondary groove Width	4.3 mm
Frequency	50
Effective air distance	2.5 mm
Number of pair poles	2
Number of turns	316
Number of grooves in each phase at each pole	4
Primary width	68.3 mm
Secondary jag width	7.14 mm

Table 5: Output values for optimal design of LLIM

Specifications	Amounts
Jag width	4 mm
Groove width	7.3 mm
Groove depth	30.1 mm
Groove width to step ratio	0.7
Secondary iron thickness	15.9 mm
Motor length	0.251 m
Frequency	50
Air gap	2.72 mm
Number of pair poles	2
Number of turns	267
Number of grooves in each phase at each pole	3
Primary width	67.21 mm

Table 6: Outputs of HLIM, LLIM, FLIM

Variables	Thrust Force (N)	Braking force (N)	Efficiency (%)	Power factor
FLIM	25.1	0.32	54.2	0.463
LLIM	27.8	0.91	65.8	0.527
HLIM	33.4	1.12	72.3	0.618

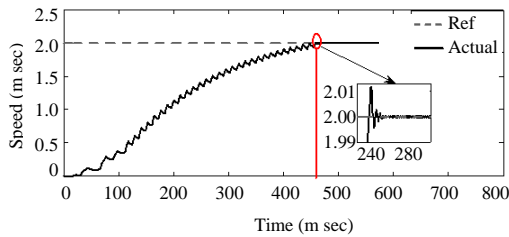


Fig. 5: Linear speed of HLIM

control of HLIM by the DTFC method. For this purpose, the reference value of LIM speed is selected 2 m sec that is equal to 7.2 km h^{-1} . For values of FLIM and LLIM, we have used the PSO algorithm and optimized them. This values listed in Table 4-6.

Figure 5-7 show HLIM, LLIM and FLIM respectively. Speed of HLIM achieving reference speed in 0.247 sec and with 0.04% ripple and speed of LLIM in 0.466 sec and 0.74% ripple, reaches the desired speed. Also, speed of FLIM reaches the desired speed in 0.618 sec and with 0.76% ripple.

Using Eq. 36-40 and according to Fig. 7-10, HLIM, LLIM and FLIM can produce 33.4, 27.8 and 25.1 N,

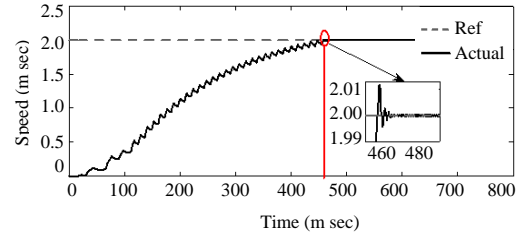


Fig. 6: Linear speed of LLIM

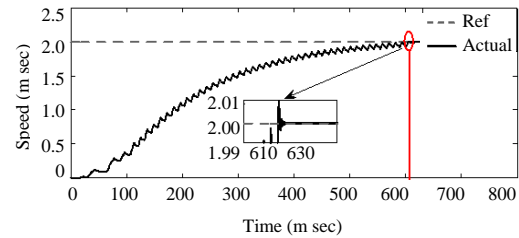


Fig. 7: Linear speed of FLIM

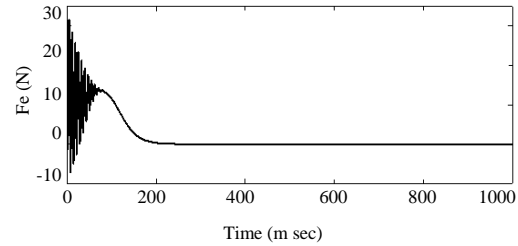


Fig. 8: Thrust force of HLIM

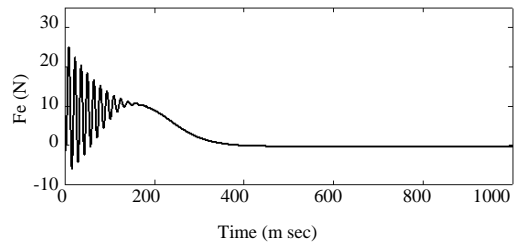


Fig. 9: Thrust force of LLIM

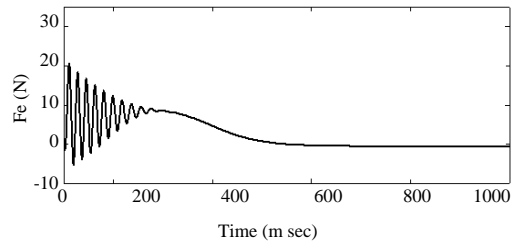


Fig. 10: Thrust force of LLIM

respectively. Also, these values obtained in the duration of 5.18 msec for HLIM, 10.4 msec for LLIM and 15.72 msec for FLIM.

As well as by Eq. 24-35, we can calculate current of HLIM, LLIM and FLIM. Also in the LIMs, the braking Force (F_b), efficiency (η) and power factor ($\cos \varphi$) are obtained by the Eq. 41-43^[3, 6]:

$$F_b = \frac{3R_{2LIM}(i_{ds} + i_{dr})^2}{2f\tau} \quad (41)$$

$$\eta = \frac{F_e V}{2f(F_e + F_b) + 3R_1 i_{ds}^2} \quad (42)$$

$$\cos\varphi = \frac{2f\tau(F_e + F_b)R_1 i_{ds}^2}{U_{ds}} \quad (43)$$

The above relationships have used for HLIM, LLIM and FLIM and the results are given in Table 6.

CONCLUSION

The Linear Induction Motors with Ladder secondary (LLIMs) have more Thrust Force than Linear Induction Motors with Flat secondary (FLIMs). However due to their higher design cost, they are less popular. In this study we proposed a Linear Induction motor with Hybrid (HLIM) secondary and its relationships with consideration of the end effect. Then, this motor optimally designed using the Particle Swarm Optimization (PSO) algorithm. Next its output speed is controlled by the Direct Thrust Force Control (DTFC) method.

According to the results, speed of HLIM reaches the desired speed in less time than and also less ripple than LLIM and FLIM. Also, HLIM has more power factor as well as more thrust force and more efficiency than LLIM and FLIM. Also, HLIM has less design cost than the LLIM and FLIM.

REFERENCES

01. Mousaei, A. and M.B.B. Shrifian, 2020. Design and optimization of a linear induction motor with hybrid secondary for textile applications. Proceedings of the 28th IEEE Iranian Conference on Electrical Engineering, May 26-28, 2020, IEEE, Tabriz, Iran, pp: 1-6.
02. Shadabi, H., A.R. Sadat, A. Pashaei and M.M.B. Sharifian, 2014. Speed control of linear induction motor using DTFC method considering end-effect phenomenon. *Int. J. Tech. Phys. Prob. Eng.*, 6: 75-81.

03. Yamazaki, K., 1997. Modification of 2D nonlinear time-stepping analysis by limited 3D analysis for induction machines. *IEEE. Trans. Magn.*, 33: 1694-1697.
04. Shiri, A. and A. Sholai, 2016. Linear induction motor, analysis, design and modeling. Shahid Rajaei University Press Education, Tehran, Iran.
05. Amiri, E. and E.A. Mendrela, 2013. A novel equivalent circuit model of linear induction motors considering static and dynamic end effects. *IEEE. Trans. Magn.*, 50: 120-128.
06. Laithwaite, E.R. and S.A. Nasar, 1970. Linear-motion electrical machines. *Proc. IEEE.*, 58: 531-542.
07. Shiri, A. and A. Shoulaie, 2012. Design optimization and analysis of single-sided linear induction motor, considering all phenomena. *IEEE. Trans. Energy Convers.*, 27: 516-525.
08. Yu, H. and B. Fahimi, 2007. Effects of airgap length variation in frictionless linear induction transportation systems. Proceedings of the 2007 IEEE Vehicle Power and Propulsion Conference, September 9-12, 2007, IEEE, Arlington, Texas, pp: 377-382.
09. Woronowicz, K. and A. Safaee, 2014. A novel linear induction motor equivalent-circuit with optimized end effect model. *Can. J. Electr. Comput. Eng.*, 37: 34-41.
10. Sarapulov, F., S. Sarapulov and I. Smolyanov, 2017. Compensated linear induction motor characteristics research by detailed magnetic equivalent circuit. Proceedings of the 2017 International Conference on Industrial Engineering, Applications and Manufacturing (ICIEAM), May 16-19, 2017, IEEE, St. Petersburg, Russia, pp: 1-4.
11. Zare-Bazghaleh, A., M.R. Naghashan and A. Khodadoost, 2015. Derivation of equivalent circuit parameters for single-sided linear induction motors. *IEEE. Trans. Plasma Sci.*, 43: 3637-3644.
12. Isfahani, A.H., B.M. Ebrahimi and H. Lesani, 2008. Design optimization of a low-speed single-sided linear induction motor for improved efficiency and power factor. *IEEE. Trans. Magn.*, 44: 266-272.
13. Hofmann, R., A. Binder and R. Pfeiffer, 2001. Investigations on a linear induction machine for railway applications. Proceedings of the IEMDC 2001 IEEE International Electric Machines and Drives Conference (Cat. No. 01EX485), June 17-20, 2001, IEEE, Cambridge, Massachusetts, pp: 20-26.
14. Fujii, N. and T. Harada, 1999. A new viewpoint of end effect of linear induction motor from secondary side in ladder type model. *IEEE. Trans. Magn.*, 35: 4040-4042.

15. Yamaguchi, T., M. Ito and K. Matsui, 1997. Improvement of thrust of linear induction motor using modified ladder slits. Proceedings of Power Conversion Conference-PCC'97 Vol. 2, August 6, 1997, IEEE, Nagaoka, Japan, pp: 563-566.
16. Naderi, P. and A. Shiri, 2018. Modeling of ladder-secondary-linear induction machine using magnetic equivalent circuit. IEEE. Trans. Veh. Technol., 67: 11411-11419.
17. Kazraji, S.M., M.R. Feyzi, M.B. Sharifian and S. Tohidi, 2017. Fuzzy Predictive Force Control (FPFC) for speed sensorless control of single-side linear induction motor. Eng. Technol. Applied Sci. Res., 7: 2132-2138.
18. Holakooie, M.H., A. Taheri and M.B.B. Sharifian, 2015. MRAS based speed estimator for sensorless vector control of a linear induction motor with improved adaptation mechanisms. J. Power Electr., 15: 1274-1285.
19. Lin, F.J., C.K. Chang and P.K. Huang, 2007. FPGA-based adaptive backstepping sliding-mode control for linear induction motor drive. IEEE. Trans. Power Electron., 22: 1222-1231.
20. Kennedy, J. and R.C. Eberhart, 1995. Particle swarm optimization. Proc. IEEE Int. Conf., 27: 1942-1948.